

## Study on Locomotion of a Crawling Robot for Adaptation to the Environment

Li Chen<sup>1</sup>, Yuechao Wang<sup>2</sup>, Bin Li<sup>2</sup>, Shugen Ma<sup>2,3</sup> and Dengping Duan<sup>1</sup>

<sup>1</sup>*Institute of Aerospace Science and Technology, Shanghai Jiaotong University,*

<sup>2</sup>*Key Robotics Laboratory, Shen Yang Institute of Automations,*

<sup>3</sup>*Organization for Promotion of the COE Program, Ritsumeikan University*  
<sup>1,2</sup> P.R. China, <sup>3</sup> Japan

### 1. Introduction

With the marriage of biomimetics and robotics, there has been a new revolution in structure design and selection of gaits of robot, and thus the field of robotic application was broadly enlarged. Crawling robot as one type of biological inspired robot has been studied in the last forty years (Hirose, 1993). The main characteristics of the crawling robot is that it has low gravity center, narrow body section and many degrees of freedom, thus it has many types of locomotion for a higher adaptability to the environment. However, in spite of a wealth of research work on the realization of their locomotion of the crawling robots (Togawa et al., 2000; Yim et al., 2000; Burdick et al., 1993), there are very few concerning the improvement of the adaptation to the environment. Therefore, two main categories of work should be stressed on: one is improvement the adaptability of an existing type of locomotion for as many different environments as possible, and the other is to lay out a new efficient type of locomotion for a specially given environment.

In our former researches (Chen et al., 2003; Chen et al., 2004) it is found that traveling wave locomotion is a widely used type of locomotion and getting over a vertical obstacle is a rigorous environment for a crawling robot. So in order to increase the environmental adaptability of a crawling robot, in this paper some studies are introduced and arranged as follows: Firstly, a new reconfigurable modular crawling robot has been developed, which can achieve some locomotion not only on a plane but also in a 3-dimensional space by different reconfiguration. Secondly, according to traveling wave locomotion, a good theoretical comprehension of this locomotion is represented based on its kinematics and dynamics analysis with the environment constrains. And some experiments are carried out to validate its high ability of environmental adaptation and improve motion efficiency. Thirdly, a new type of locomotion, namely rolling locomotion, is proposed to get over an obstacle. It is interesting that three kinds of lateral rolling locomotion are realized, through which a crawling robot can achieve net lateral translation, alternation of the contact subspace and crossing over some obstacles only with a few models.

Source: Bioinspiration and Robotics: Walking and Climbing Robots, Book edited by: Maki K. Habib  
 ISBN 978-3-902613-15-8, pp. 544, I-Tech, Vienna, Austria, EU, September 2007

## 2. Mechanism of the Developed Crawling Robot

The modular unit of the crawling robot is shown in Fig.1 (a), each module is 7cm×3.3 cm×5.5cm and its weight is 0.1kg. It is mainly equipped with a motor, a motor housing and an active board. The motor, which is fixed on the box-like motor housing, is a small-g geared DC motor which provides closed-loop position control. The rotation can be transmitted from one module to its connecting module through the active board. This direct driving unit is light, simple and robust. When the one-DOF modules are connected in parallel, every module acts as a one-DOF joint; and when the one-DOF modules are connected perpendicularly, every two adjacent modules act as a two-DOF combined joint, as shown in Fig.1 (b).

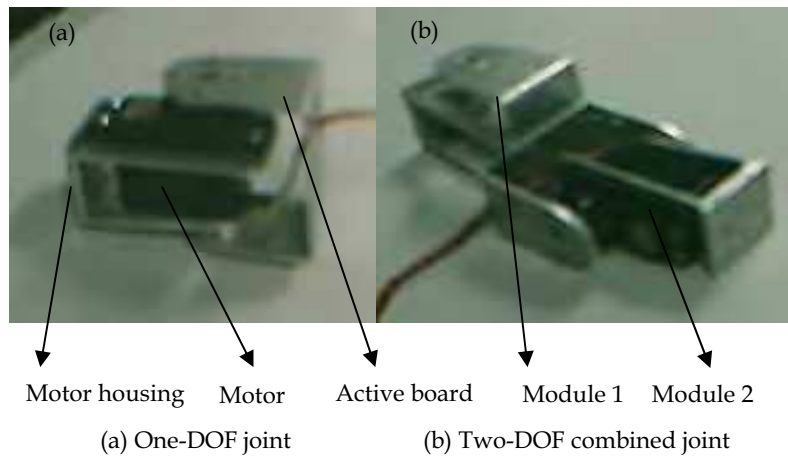


Figure 1. Two types of joints

The whole robot is consisted of nine modules and one head, which is equipped with a controller. Two configurations of the crawling robot can be obtained: planer configuration (when it is connected with one-DOF joint) as shown in Fig.2 (a), and spatial configuration (when it is connected with two-DOF joint) as shown in Fig.2 (b). The planer configuration can be used to realize some planar locomotion with wheels at a high speed, and the spatial configuration can be used to achieve complex 3-dimensional locomotion without wheels.

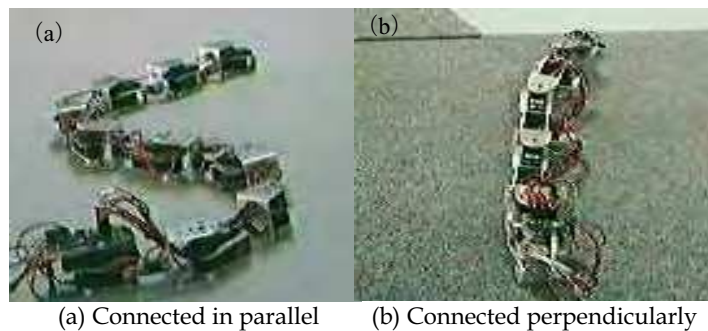


Figure 2. Crawling robot in different configurations

Fig.3 illustrates the general control architecture of our crawling robot. Motion planning is accomplished in a PC computer. The motor driver and the CPU board are mounted on the head of the crawling robot. Two voltages (9V for logic circuits on the motor driver and the CPU board and 5 V for driving the motor) are supplied through cables. Serial Servo Controllers use a computer's serial port to control standard radio-control (R/C) servos up to eight servos. The servo is responsible for maintaining the position through its own feedback control systems. This provides servo motion and control from one extreme to the other.

Learning from the past experiments in crawling robots (Ma., 2002), we choose the parallel control strategy for the locomotion in three-dimensional, in which the joint angles are represented separately at each time step. Our crawling robot's locomotion is generated by adjusting the joint variables simultaneously and separately in a time step. This kind of control method can form smoother body curve and thus generate the accelerated or decelerated locomotion.

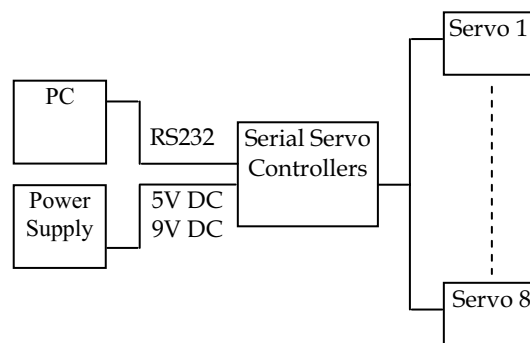


Figure 3. General control architecture

### 3. Dynamic Analysis of Traveling Wave Locomotion

Two main planar models, serpentine locomotion (horizontal locomotion) and traveling wave locomotion (vertical locomotion) are often adopted in crawling robot (Paap et al., 1996; Ma et al., 2002; Poi, 1998; Chen, 2003). The serpentine locomotion is formed in the supporting plane, and its driving forces result from the different friction coefficients of the body in the tangential and the normal directions with respect to the supporting plane (Dowling, 1997; Yim, 1994). So the locomotors usually need wheels to realize the directional friction and hence the adaptability to the environment was somewhat weakened. On the contrary, traveling wave locomotion developed in vertical plane orthogonal to the supporting plane has more substantial potential for adaptability to the environment without additional consideration of the friction condition.

However, the traveling wave locomotion is always characterized as a low efficient gaits (Chirikjian and Burdick, 1995) because till to now its dynamics is somewhat obscure (Prautsch and Mita, 1999; Saito, 2000) and only based on kinematic analysis no effective controlling methods can be conducted. In this section starting with the dynamic model, simulation and finishing with experiment, a systematic complete description of traveling wave locomotion is conducted for a good comprehension and higher efficiently controlling this gait.

### 3.1 Kinematics and Dynamics with Environment Constraints

Consider the link model of crawling robot as shown in Fig. 4, each link  $i$  has its own local coordinate system  $o_i-x_i-z_i$  on the joint. In addition, there is a base frame  $O-X-Z$ . If  $O-X-Z$  is fixed in the inertial frame, take the  $(i+1)$ th link of the crawling robot for example, the position, velocity and acceleration of gravity center of link  $i$  can be derived as follows in the case of assuming the uniform link:

$$x_{iG} = x_i + l/2 \cos \phi_i \quad (1)$$

$$z_{iG} = z_i + l/2 \sin \phi_i \quad (2)$$

$$\dot{x}_{iG} = \dot{x}_i - l/2 \sin \phi_i \dot{\phi}_i \quad (3)$$

$$\dot{z}_{iG} = \dot{z}_i + l/2 \cos \phi_i \dot{\phi}_i \quad (4)$$

$$\ddot{x}_{iG} = \ddot{x}_i - l/2 \cos \phi_i \dot{\phi}_i^2 - l/2 \sin \phi_i \ddot{\phi}_i \quad (5)$$

$$\ddot{z}_{iG} = \ddot{z}_i - l/2 \sin \phi_i \dot{\phi}_i^2 + l/2 \cos \phi_i \ddot{\phi}_i \quad (6)$$

$$i = 1, 2, \dots, n$$

where  $x_{iG}$  and  $z_{iG}$ ,  $\dot{x}_{iG}$  and  $\dot{z}_{iG}$ ,  $\ddot{x}_{iG}$  and  $\ddot{z}_{iG}$  represent the position, velocity and acceleration of gravity center of the  $i$ th link along  $X$  and  $Z$  axis. Using the equations (1)-(6), the position, velocity and acceleration of gravity center of the crawling body can be obtained as follows:

$$X_G = \frac{\sum_{i=1}^n m_i x_{iG}}{M} = \frac{1}{n} \sum_{i=1}^n x_{iG} \quad (7)$$

$$\dot{X}_G = \frac{\sum_{i=1}^n m_i \dot{x}_{iG}}{M} = \frac{1}{n} \sum_{i=1}^n \dot{x}_{iG} \quad (8)$$

$$\ddot{X}_G = \frac{\sum_{i=1}^n m_i \ddot{x}_{iG}}{M} = \frac{1}{n} \sum_{i=1}^n \ddot{x}_{iG} \quad (9)$$

$$Z_G = \frac{\sum_{i=1}^n m_i z_{iG}}{M} = \frac{1}{n} \sum_{i=1}^n z_{iG} \quad (10)$$

$$\dot{Z}_G = \frac{\sum_{i=1}^n m_i \dot{z}_{iG}}{M} = \frac{1}{n} \sum_{i=1}^n \dot{z}_{iG} \quad (11)$$

$$\ddot{Z}_G = \frac{\sum_{i=1}^n m_i \ddot{z}_{iG}}{M} = \frac{1}{n} \sum_{i=1}^n \ddot{z}_{iG} \quad (12)$$

where  $X_G$  and  $Z_G$ ,  $\dot{X}_G$  and  $\dot{Z}_G$ , and  $\ddot{X}_G$  and  $\ddot{Z}_G$  represent the position, velocity and acceleration of gravity center of the crawling body along X and Z axis respectively.

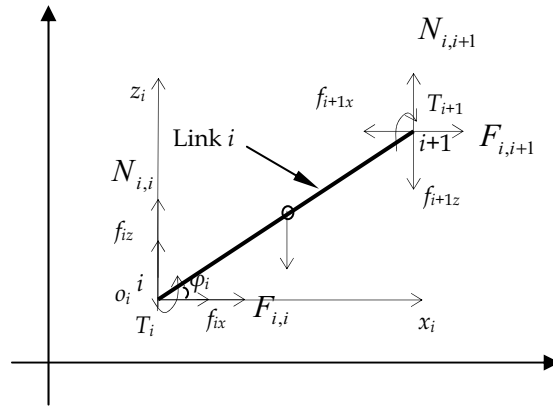


Figure 4. Scheme of forces acted on the  $i$ th link

The dynamics of the crawling robot can be viewed as a combination of mechanism dynamics and environment constraints. The objective of mechanism dynamics is to model the functional relationship between the joint torques and the robot locomotion. Whereas, the interaction force between the body and the environment can be determined by environment constraints.

The force diagram of the  $i$ th link is also illustrated in Fig.4, where  $N_{i,i+1}$  and  $F_{i,i+1}$  are the supporting force and friction force of the  $i$ th link at the  $(i+1)$ th joint,  $T_i$ ,  $f_i$ ,  $m_i$  and  $I_i$  represent the torques, internal forces, mass and moment of inertia of the  $i$ th link, respectively. Therefore, based on the principle of the Newton, the motion for the  $i$ th link with respect to the  $(i+1)$ th link can be described:

$$f_{ix} - f_{i+1x} + F_{i,i} + F_{i,i+1} = m\ddot{x}_{iG} \quad (13)$$

$$f_{iz} - f_{i+1z} + N_{i,i} + N_{i,i+1} - mg = m\ddot{z}_{iG} \quad (14)$$

$$\tau_i - \tau_{i+1} + (f_{ix} + f_{i+1x} + F_{i,i} - F_{i,i+1})l \sin \phi_i / 2 - (f_{iz} + f_{i+1z} + N_{i,i} - N_{i,i+1})l \cos \phi_i / 2 = I_i \ddot{\phi}_i \quad (15)$$

Since the head and tail of the crawling robot are free, there are two equations:

$$f_{1x} = f_{1z} = f_{n+1x} = f_{n+1z} = 0 \quad (16)$$

$$\tau_1 = \tau_{n+1} = 0 \quad (17)$$

From the equations (13), (14) and (16), we can obtain:

$$\sum_{i=1}^n m\ddot{x}_{iG} = \sum_{i=1}^{n+1} F_i \quad (18)$$

$$\sum_{i=1}^n m\ddot{z}_{iG} = 0 \quad (19)$$

Substituting equations (5) and (6) into equations (18) and (19) we obtain:

$$m\ddot{x}_1 - \sum_{i=1}^n \left[ \sum_{k=1}^{i-1} (l \cos \phi_k \dot{\phi}_k^2 + l \sin \phi_k \ddot{\phi}_k) + \frac{l}{2} \cos \phi_i \dot{\phi}_i^2 + \frac{l}{2} \sin \phi_i \ddot{\phi}_i \right] = \sum_{i=1}^{n+1} F_i \quad (20)$$

$$n\ddot{z}_1 - \sum_{i=1}^n \left[ \sum_{k=1}^{i-1} (l \sin \phi_k \dot{\phi}_k^2 - l \cos \phi_k \ddot{\phi}_k) + \frac{l}{2} \sin \phi_i \dot{\phi}_i^2 - \frac{l}{2} \cos \phi_i \ddot{\phi}_i \right] = 0 \quad (21)$$

The equations (20) and (21) represent the relation between the acceleration of head (link 1)

$\ddot{x}_1$ ,  $\ddot{z}_1$  and the angular acceleration  $\ddot{\phi}_1$ .

Using the recursive formulas in equations (13) and (14), from the tail to the head the relation between the internal force and external force of every link are obtained:

$$f_{xi} = \sum_{j=i}^n m\ddot{x}_j - \sum_{j=i+1}^{n+1} F_j - F_{i,i} \quad (22)$$

$$f_{zi} = \sum_{j=i}^n m\ddot{z}_j - \sum_{j=i+1}^{n+1} N_j - N_{i,i} + (n+1-i)mg \quad (23)$$

Substituting equations (22) and (23) into torques equation (15), we have:

$$\tau_i - \tau_{i+1} + (2 \sum_{j=i}^n m\ddot{x}_j - 2 \sum_{j=i+1}^n F_j - m\ddot{x}_i) l s \phi_i / 2 - (2 \sum_{j=i}^n m\ddot{z}_j - 2 \sum_{j=i+1}^n N_j - m\ddot{z}_i + (2n+1-2i)mg) l c \phi_i / 2 = I_i \ddot{\phi}_i \quad (24)$$

where  $F_j$  and  $N_j$  represent the friction force and supporting force of the  $j$ th joint and they meet the following equations:

$$F_j = F_{j-1,j} + F_{j,j} \quad (25)$$

$$N_j = N_{j-1,j} + N_{j,j} \quad (26)$$

where  $F_i$  and  $N_i$  can be calculated from the environment constraints in the next section.

From equation (24) we obtain:

$$\sum_{i=1}^n \left\{ (2 \sum_{j=i+1}^n m\ddot{x}_j - 2 \sum_{j=i+1}^n F_j + m\ddot{x}_i) l \sin \phi_i / 2 - \left[ 2 \sum_{j=i+1}^n m\ddot{z}_j - 2 \sum_{j=i+1}^n N_j + m\ddot{z}_i + (2n+1-2i)mg \right] l \cos \phi_i / 2 \right\} = \sum_{i=1}^n I_i \ddot{\phi}_i \quad (27)$$

Equation (27) is a linear equation with one unknown variable  $\ddot{\phi}_1$ . Solving equation (27), the rotation acceleration of the first joint  $\ddot{\phi}_1$  can be obtained, and then substituting it into

equations (20) and (21), the linear acceleration of head (link1)  $\ddot{x}_1, \ddot{z}_1$ , can be correspondingly derived. The rotation velocity and angle, and moving velocity and position of first joint can be obtained through integration. Substituting these values into equation (24), the joint torques required to generate the robot motion are obtained.

Main subject of dynamics with environment constraints is to calculate the interaction forces between the environment and the crawling body. Because the supporting force and friction force from the environment on the crawling body is a function of the body shape in the traveling wave locomotion, a crawling robot with the  $n=16$  segments and the shape number of the body  $K_n=2$  is taken as example.

Fig.5 shows the traveling wave in one segment, where it has at least two supporting points with the ground. The joints contacting the ground are set as  $u$  and  $u'$ . If the gravity center of the body is located within the supporting points, the wave shape would be stable. External forces acting on the crawling body are the gravity force  $G$ ; supporting force  $N$  and friction force  $F$ . Gravity force and supporting force are balanced, so the resultant force is the friction force, which is the driving force. Based on the force and moment balance, we can obtain

$$N_u = \frac{1}{\lambda} [(G + M\ddot{Z}_G)(x_G - x_{u'}) - M\ddot{X}_G z_G] \quad (28)$$

$$N_{u'} = G - N_u \quad (29)$$

where  $\lambda$  is the distance between the two supporting points,  $M\ddot{X}_G$  and  $M\ddot{Z}_G$  are the inertial forces of the body along the X-axis and Z-axis. In this study the viscous friction is neglected, and the coulomb friction is used to depict the environment dynamics:

$$F_i = -\mu \cdot \text{sgn}(v) \cdot N_i \quad (30)$$

where  $\mu$  is the friction coefficient between the contacting joint and the supporting plane. From the equations (30), (29) and (28) we can see that the driving force, i.e. the friction force is related with the position and acceleration of the robot body. So the crawling robot can be controlled by its body shape and joint torques according to its kinematics and mechanism dynamics jointly. In next section we will give some simulation results on the relationship of the joint torques, the body shape and the environmental coefficient.

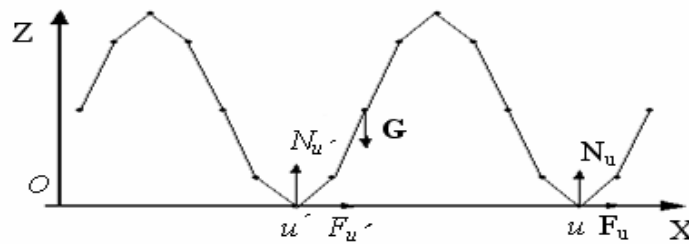


Figure 5. External forces on the snake body

### 3.2 Simulation analysis and calculation

Simulation parameters are set as follows:  $L=1.6\text{m}$ ,  $n=16$ ,  $l=0.1\text{m}$ ,  $m=0.1\text{kg}$ ,  $I=0.0001\text{kg}\cdot\text{m}^2$ ,  $g=9.8\text{N/kg}$  and  $K_n=2$ . The body shape changes with respect to the displacement of the tail along the serpenoid curve, the acceleration of  $s$  is given as follows:

$$\ddot{s} = \begin{cases} a & 0 \leq t < T/10 \\ 0 & T/10 \leq t < 9T/10 \\ -a & 9T/10 \leq t < T \end{cases} \quad (31)$$

where  $a=0.0625\text{ m/s}^2$ , locomotion time  $T=32\text{ s}$ , initial positions are selected as  $x_1=0$ ,  $z_1=0$ , initial velocities are set as  $\dot{x}_1=0$ ,  $\dot{z}_1=0$ ,  $\dot{\phi}_1=0$ , and the initial winding angle  $\phi_1=\alpha$ .

When the friction coefficient  $\mu=0.3$ , the initial winding angle of body shape  $\alpha=\pi/6$ , the changes of the torques in joint 3, 7, 9, 13 are shown in Fig.6. From Fig.6 we can see: 1) the required torque for each joint in traveling wave locomotion is periodic, 2) Torques in edge joint 3 and joint 13 are small, in joint 7 is larger and in central joint 9 is the biggest, that is because joint 3 and 13 have a longer distance from gravity center than joint 7 and joint 9. The total  $n$  is 16, and the joint 9 has the nearest distance from the gravity center, thus the biggest joint torque output of joint 9 is the biggest torque output of the crawling robot. In a word, the input torque of each joint will decrease while the distance between the joint and the center of gravity of the body increases, and the biggest input torque is that of the central joint.

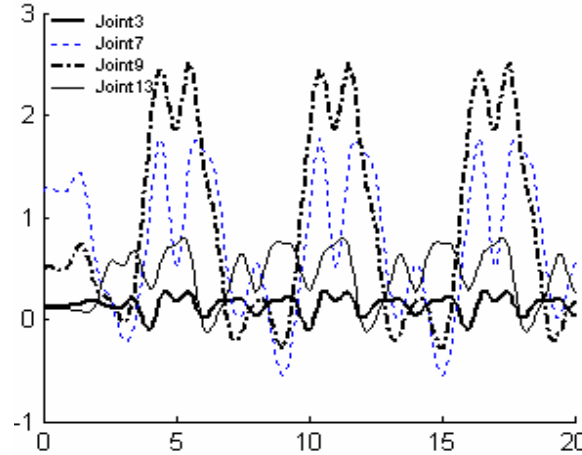


Figure 6. Variation of joint torques ( $\mu=0.3$ ,  $\alpha=\pi/6$ )

Variations of symmetrical joint torques can be seen from Fig.7. Symmetrical joint 3 and 15, 7 and 11 have the same distance from the gravity center, and except a phase difference the amplitude variations of the input torques are the same.

Joint 9 is taken to study the effect of variation of the friction coefficient with the environment  $\mu$  on the joint torques. As seen in Fig. 8, when  $\alpha=\pi/6$ , and  $\mu$  is chosen as 0.1, 0.3, 0.5 and 0.7 respectively, keeping the initial angle invariable, the joint input torques are increased with the increasing of friction coefficient with the environment. By the way, it can be found that there is difference of torque characteristics for with others. It is because that the friction



coefficient is closely related to energy consumption in vertical locomotion. The average power consumption per unit distance  $E$  can be calculated using Eq. (32) as:

$$E = \frac{\sum_{i=1}^n \int_0^T |\tau_i \omega| dt}{L_{dist}} \tag{32}$$

in which  $L_{dist}$  is the linear distance moved in a same period  $T$ . The calculating results when  $\mu$  is specified as 0.1, 0.3, 0.5, 0.7 and 0.9 respectively are summarized in Tab.1. It can be found from Tab.1 that the crawling robot has the lowest energy consumption when  $\mu=0.3$  which makes its torque characteristic different from others.

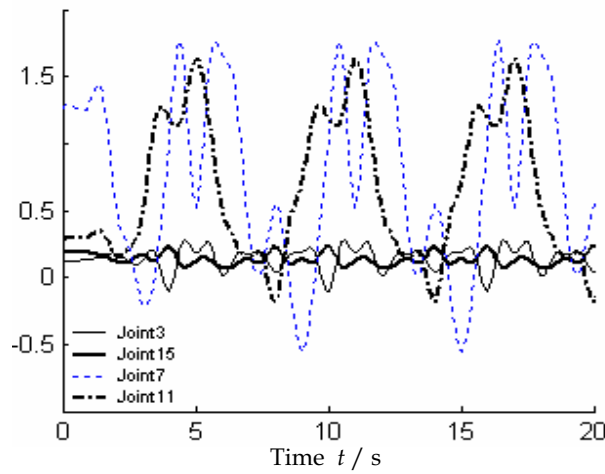


Figure 7. Variation of symmetry joint torque ( $\mu=0.3, \alpha=\pi/6$ )

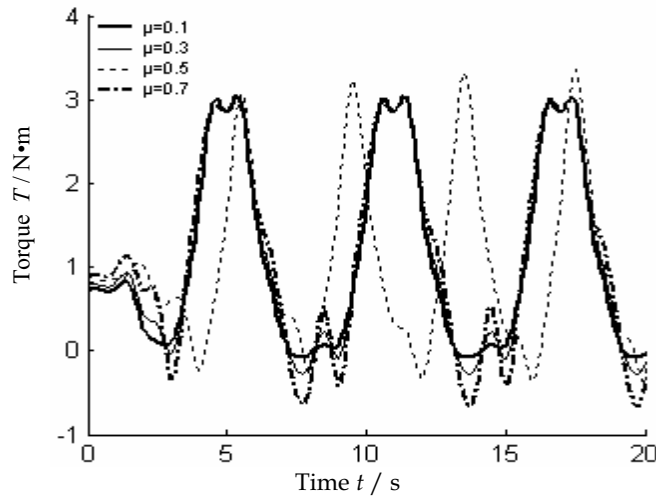


Figure 8. Effect of environment on the joint torques

$\mu$	$\mu = 0.1$	$\mu = 0.3$	$\mu = 0.5$	$\mu = 0.7$	$\mu = 0.9$
E(N m)	430	380	320	500	700

Table 1. Power consumption per unit distance varying with friction coefficient

Also joint 9 is taken to investigate the effect of variation of the initial winding angle on the joint torques. As seen in Fig 9, when  $\mu=0.5$ , and  $\alpha$  is chosen as  $\pi/12$ ,  $\pi/6$ ,  $\pi/4$  and  $\pi/3$  respectively, keeping the friction coefficient with the environment invariable, the joint input torques are decreased with the increasing of the initial winding angle. So if friction coefficient with the environment is big, and the maximum joint torque exceeds the maximum input torque value of the motor, accordingly the initial winding angle can be increased to reduce the input torque required for locomotion.

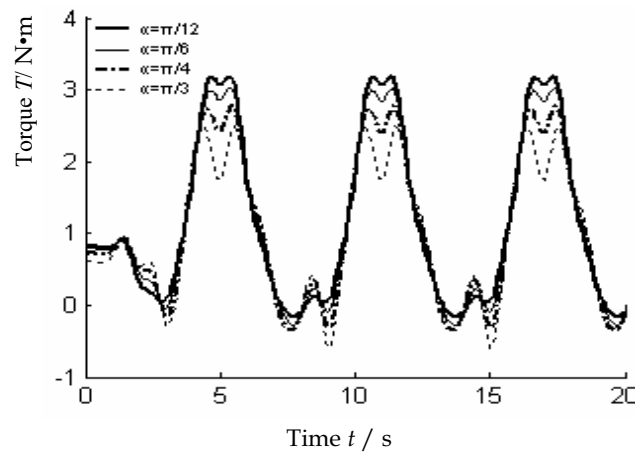
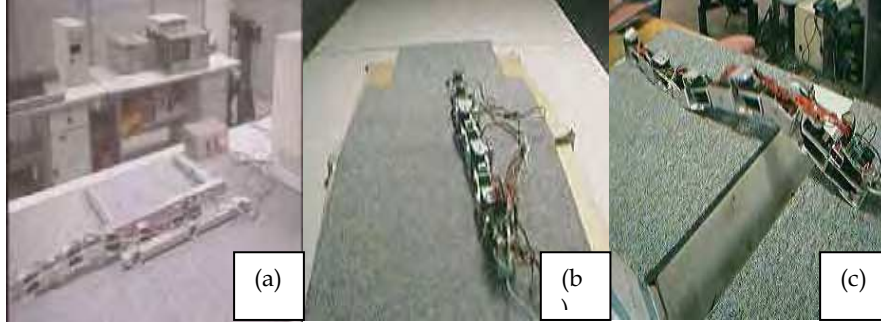


Figure 9. Effect of initial winding angle on the joint torques

### 3.3 Experimental Validation

Some experiments were conducted under different environments. Fig.10 (a) shows the robot going through a narrow space on a flat carpet, where the friction coefficient is 0.3, the initial winding angle  $\alpha$  is 0.4 rad, the maximum joint output torque is  $0.5\text{N}\cdot\text{m}$ . Fig.10 (b) shows the robot climbing on the same carpet with a slope of 20 degree, which means increasing the friction coefficient to  $\mu=0.7$ , on the same condition of the initial winding angle  $\alpha=0.4$  rad, the maximum joint output torque is increased to  $0.82\text{N}/\text{m}$ . This validates the simulation results that keeping the initial angle invariable, the joint input torques are increased with the increasing of friction coefficient. Fig.10(c) shows the robot is crossing a gap. If the initial winding angle is kept as  $\alpha=0.4$  rad, the robot can not provide the output torque high enough to lift its head to reach the other edge of gap, but when the initial winding angle is increased to  $\alpha=0.75$  rad, the maximum wideness of gap that can be crossed is 0.14 m. This also is well in accordance with the simulation results that increasing the initial winding angle can reduce the maximum joint torque.



(a) going through a narrow space (b) climbing a slope (c) crossing a gap  
Figure 10. Traveling wave locomotion of snake robot

#### 4. Lateral Rolling Locomotion for getting over the obstacle

Yim demonstrated that his crawling robot can cross over a bar by using caterpillar like locomotion and rolling track (Yim., 1994). But the caterpillar like locomotion depends on the difference of the static and sliding friction forces between the crawling body and the ground, so the crawling robot need a large number of modules to provide enough driving forces during crossing, while the rolling track has low stability on the obstacles, so it is bounded by the appearance of the obstacles.

In this section a new 3-dimensional locomotion, lateral rolling, is proposed for this crawling robot to cross over obstacles. The attractive characteristic of the lateral rolling locomotion is that it can move on smoother surface just with a few modules, and can also cross many types of obstacles.

##### 4.1 Control of Lateral Rolling Locomotion of the crawling robot

As shown in Fig.11, a simplified model is introduced for the articulated crawling robot in spatial configuration. Two groups of control signals  $\Theta = [\theta_1, \theta_2, \dots, \theta_m]$  and  $\Phi = [\varphi_1, \varphi_2, \dots, \varphi_m]$  are represented the relative joint angles around the pitch axis and yaw axis respectively, where  $m$  is the number of the combined joints.

Hirose studied crawlings and found that their bodies take on the so-called serpenoid curve when they move with a serpentine gait on a plane and Ma (Ma et al, 2002) derived the symbol expression of relative rotate angle between two adjacent modules. Based on these, in this study the 3-dimensional locomotion curve is described by the composition of the horizontal serpenoid curve from the bending angles around yaw axis and the vertical serpenoid curve from the bending angles around pitch axis. The control signals of 3-dimensional gaits are thus proposed as follows:

$$\begin{cases} \theta_i(s) = -2\alpha_{\theta_0} \sin\left(\frac{K_n\pi}{n_\theta}\right) \cdot \sin\left(\frac{2K_n\pi}{L}s + \frac{2K_n\pi}{n_\theta}i\right) \\ \phi_i(s) = -2\alpha_{\phi_0} \sin\left(\frac{K_n\pi}{n_\phi}\right) \cdot \sin\left(\frac{2K_n\pi}{L}s + \frac{2K_n\pi}{n_\phi}i + \delta\phi\right) \end{cases} \quad (33)$$

$i = 1, 2, \dots, m$

where  $\alpha_{\theta_0}$  and  $\alpha_{\phi_0}$  are the initial winding angles of two waves,  $n_\theta$  and  $n_\phi$  are the numbers of joints in each locomotion plane,  $s$  is the displacement of tail along the serpenoid curve,  $K_n$  is the number of the wave shape,  $i$  is the number of  $i$ th link,  $L$  is the whole length of the robot body,  $\delta\phi$  is the phase difference between two waves out of phase respectively. The sidewinding locomotion of crawling robot will be generated by controlling  $\theta$  and  $\phi$  according to the Equation.33. The lateral rolling is a 3-dimensional locomotion without crawling-like movements. The body shape curve is also can be described by the composition of the bending motions around yaw axis and pitch axis, but without changing along the body shape curve, i.e. the phase difference between every two joints is zero. Hence equation.33 can be rewritten as follows:

$$\begin{cases} \theta_i(s) = -2\alpha_{\theta_0} \sin\left(\frac{K_n\pi}{n_\theta}\right) \cdot \sin\left(\frac{2K_n\pi}{L_\theta} s\right) \\ \phi_i(s) = -2\alpha_{\phi_0} \sin\left(\frac{K_n\pi}{n_\phi}\right) \cdot \sin\left(\frac{2K_n\pi}{L_\phi} s + \delta\phi\right) \end{cases} \quad (34)$$

where the number of modules  $n_\theta$ ,  $n_\phi$  and the length of the body  $L$  are determined by the mechanical structure. The displacement  $s$  of the tail along the serpenoid curve, which determines the changing frequency of the body curve, is given by user. The amplitudes  $\alpha_{\theta_0}$  and  $\alpha_{\phi_0}$ , the phase difference  $\delta\phi$  and wave number  $K_n$  are the control variables.

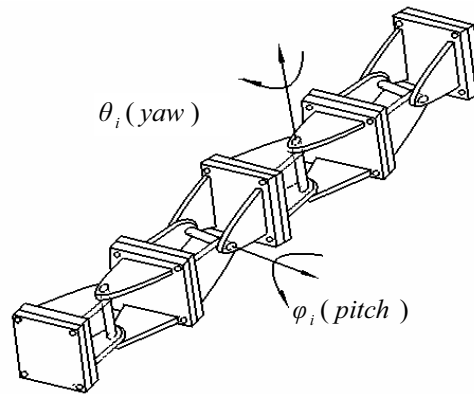


Figure 11. Control model of the two-DOF joints

#### 4.2 Experimental of rolling over obstacles

The whole body length is 0.7m long, so that the parameter  $L$  in Equation 34 is 0.7m. Four combined joints are divided alternatively into two planes, namely each four in one plane, i.e.

$n_\theta = n_\phi = 4$ , which is the minimum number to form one wave in a plane, thus the value of the parameter  $K_n \leq 1$ .

Experimental results show that when the difference phase is  $\pm\pi/2$ , the robot locomotion has high stability. Under this condition and when the frequency  $s$  is given, three types of lateral rolling locomotion, flapping, linear rolling and curved rolling can be achieved by controlling the amplitudes and the number of the two waves, as shown in Fig.12.

If the amplitudes is low (e.g.  $\alpha_{\theta_0} = \alpha_{\phi_0} = \pi/18$ ) and the wave number  $K_n$  is 1, this mode uses in-phase motions of the ends to swing forward, then the ends come down in contact with the ground and the center of the body is lifted or dragged forward, namely the flapping locomotion, as shown in Fig.12 (a). Using this flapping locomotion the crawling robot can realize net lateral translation.

If the amplitudes is higher (e.g.  $\alpha_{\theta_0} = \alpha_{\phi_0} = \pi/6$ ) and the  $K_n$  is set less than 1 (e.g.  $K_n = 0.5$ ), which means the robot does not form a whole wave, this mode makes the crawling robot rolling over the ground with almost every joint touching the ground, we name it as linear rolling, as shown in Fig.12 (b). Using this linear rolling the crawling robot can change its contact base for various types of locomotion or recover from overturn.

If the amplitudes is high enough (e.g.  $\alpha_{\theta_0} = \alpha_{\phi_0} = \pi/3$ ) and keep  $K_n = 1$ , then the composition of the two former locomotion is obtained, that is to say, the ends and the center of the robot body alternatively contact the ground while rolling, we name it as curved rolling, as shown in Fig.12 (c). Using this curved locomotion the robot can cross over some obstacles while lateral to it, as shown in Fig.13. The bar obstacle that the crawling robot is rolling over is 8cm high. Locomotion speed is about 4cm/s. Fig.13 (a) is the initial state, (b) is the stage of forming the initial wave shape, (c) shows some modules have left off the ground, (d) is the state that the robot begins to cross over the obstacle, (e) is the state where the robot is over the obstacle, (f) shows the state that the robot is leaving the obstacle, (g) gives the state that the robot has left from the obstacle and (h) shows the robot to go ahead, respectively.

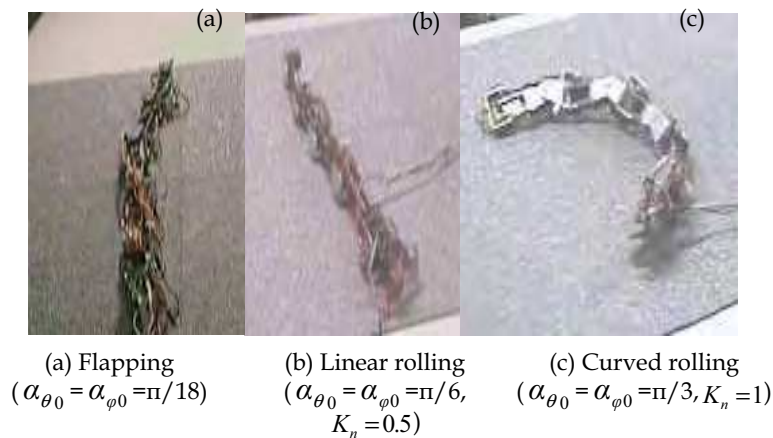


Figure 12. Lateral locomotion of the snake robot

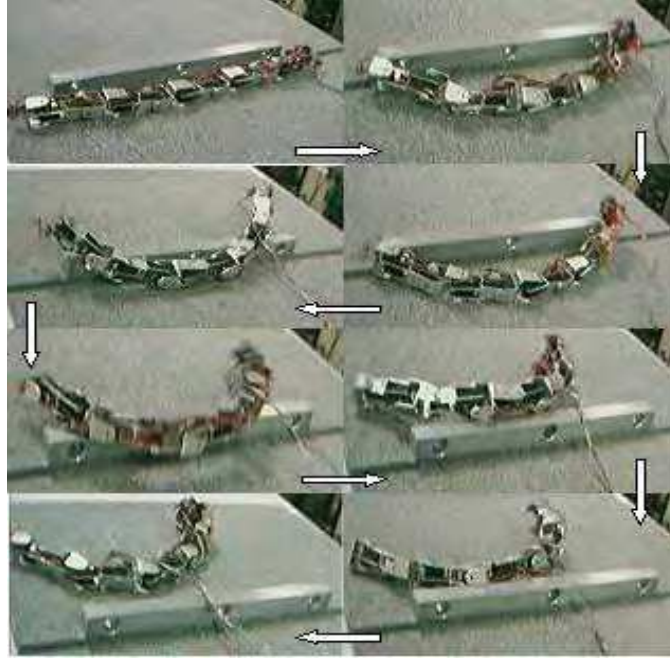


Figure 13. Rolling over an obstacle of the snake robot

#### 4.3 Discussion

The results show that the curved rolling shape and direction depend on the transferring directions and phase difference of the two waves respectively. The body of crawling forms a curve during rolling and the transferring directions of the two waves in different planes determine the shape. The rolling direction is orthogonal to the body axis. The phase difference determines whether the robot rolls along the inside direction or the outside of the curve. The phase difference and transferring directions and their effect on the rolling shape and direction are shown in Tab.1, where '+' means the wave is traveling from the tail to the head and '-' means the wave is traveling from the head to the tail. When the phase difference is  $\pi/2$ , the direction of motion is along the inside normal, and vice versa.





Phase difference	$\pi/2$	$\pi/2$	$-\pi/2$	$-\pi/2$
Transferring directions of waves	+	-	+	-
Body-shape and its rolling direction				

Table 2. The influence of phase difference and transferring directions of waves on the body-shape and direction of rolling

It is also clear that the rolling locomotion obtains its driving force from interaction with its environment, but not from the special friction condition between the body and the ground as serpentine locomotion. The interaction depends on the variation of adjacent joint rotate angles of the two waves. During one period, the variation of rotate angles around yaw axis and pitch axis can be plot according to the control equations.2, as shown in Fig.7. The angle  $\theta_i$  around the yaw axis first varies from zero to positive maximum, next to zero, then to negative maximum and at last return to the zero position, accordingly the angle  $\phi_i$  around the pitch axis varies from negative maximum to zero, next to positive maximum, then to zero and at last return to the negative maximum. That is when the rotate angle around the pitch axes  $\phi_i$  is the maximum, the rotate angle around the yaw axis  $\theta_i$  is zero, and vice versa. This regularity leads to the best drive force during rolling.

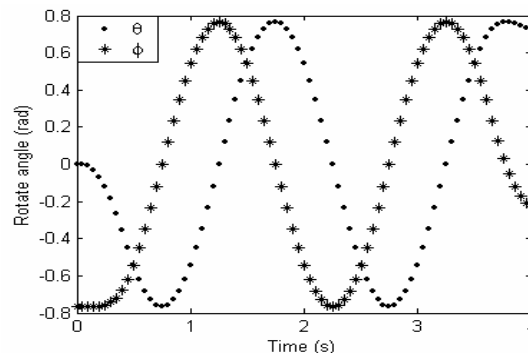


Figure 14. Variation of adjacent joint rotate angles during one period

## 5. Conclusion

The motivation of this research is to improve the locomotion adaptation to the environment of a crawling robot:

Firstly, a new reconfigurable modular crawling robot has been developed, which can not only move on a plane but also achieve some 3-dimensional motions while reconfigured.

Secondly, the kinematic analysis combined with dynamics is taken to revise the motion mechanism of traveling locomotion for better adaptation to the environment. It is found that the adaptability of locomotion is close related with the environment parameters and the body shape: when keeping the initial winding angle unchanged, the bigger the friction coefficient with the environment is, the bigger is the joint input torque for each of joints. Whereas, while keeping the friction coefficient with the environment unchanged, the bigger the initial winding angle is, the smaller is the joint input torque for each of joints. Experiment validates the high ability of environment adaptation of the traveling locomotion and the motion efficient can be improved by dynamic analysis.

Thirdly, control equations of a new 3-dimensional lateral rolling locomotion were developed by the composition of two bending motions in mutual orthogonal plane. Three types of lateral rolling locomotion, flapping, linear rolling and curved

rolling, were achieved by controlling the amplitudes and the number of two waves in the two bending motions. The lateral rolling locomotion obtains its driving force through the interaction with the environment, and the rolling shape and its direction depend on the transferring direction and phase difference of the two waves respectively. Using these types of locomotion the snake robot can realize net lateral translation, alternation of the contact base and cross over some obstacles with a few models.

This paper can give some hints for efficiently control the locomotion of crawling robot for improvement its environmental adaptability.

## 8. References

- Burdick J, Radford J. and Chirikjian G. S., (1993). A Sidewinding Locomotion Gait for Hyper-Redundant Robots, *Advanced Robotics*, Vol.9, No, 3, pp.195-216
- Chen L., Wang Y.C., Ma S.G. and Li B., (2003). Analysis of the traveling wave locomotion of crawling robot, in *Proc. IEEE Int. Conf. on Robotics, Intelligent Systems and Signal processing*, pp, 365-369
- Chen L., Wang Y.C., Ma S.G., (2004). Studies on Lateral Rolling Locomotion of a Crawling Robot, in *Proc. IEEE Int. Conf. on Robotics and Automation*, pp, 5070-5074
- Chirikjian and Burdick ,(1995), The Kinematics of Hyper-Redundant Robot Locomotion, *IEEE Trans. on Robotics and Automation*, Vol. 11, No. 6, pp, 781-793
- Dowling K., (1997) . Limbless Locomotion: Learning to Crawl with a Crawling Robot, *Doctoral dissertation*, tech. report CMU-RI-TR-97-48, Robotics Institute, Carnegie Mellon University
- Gray J., (1946), The mechanism of locomotion in crawlings, *Journal of experimental biology*
- Hirose S., (1993). Biologically Inspired Robots (Crawling-like Locomotor and Manipulator), Oxford University Press, ISBN 0198562616, New York, United States
- Ma S., Araya H. and Li L., (2002). Development of a creeping locomotion of crawling-like robot, *Int. J. of Robotics and Automation*, vol.17, No.4, pp.146-153
- Mori M. and Hirose S., ( 2001). Development of Active Cord Mechanism ACM-R3 with Agile 3D Mobility, in *Proc. IEEE Int. Conf. on Intelligent Robots and Systems*
- Paap K. L., Dehlwisch M. and Klaassen B., (1996). GMD-Crawling: A Semi-Autonomous Crawling-like Robot, *Distributed Autonomous Robotic Systems 2*, Springer-Verlag, Tokyo
- Poi G., Scarabeo C. and Allotta B., (1998).Traveling wave locomotion hyper-redundant mobile robot, in *Proc. IEEE Int. Conf. on Robotics and Automation*
- Prautsch P. and Mita T., (1999).Control and Analysis of the Gait of Crawling robots, in *Proc. IEEE Int. Conf. on Control applications*, pp, 502-507
- Saito M., Fukaya M., and Iwasaki T., (2000). Serpentine locomotion with robotics crawlings, *IEEE control systems magazine*, Vol.20, No, 2, pp, 64-81
- Togawa K., Mori M. and Hirose S., (2000). Study on 3-dimensional Active Cord Mechanism: Development of ACM-R2, in *Proc. IEEE Int. Conf. on Intelligent Robots and Systems*
- Yim. M., (1994). New Locomotion Gains, in *Proc. IEEE Int. Conf. on Robotics and Automation*, pp, 310-316
- Yim M., Duff D.G. and Roufas K.D., ( 2000). Polybot: a Modular Reconfigurable Robot, in *Proc. IEEE Int. Conf. on Robotics and Automation*





## **Bioinspiration and Robotics Walking and Climbing Robots**

Edited by Maki K. Habib

ISBN 978-3-902613-15-8

Hard cover, 544 pages

**Publisher** I-Tech Education and Publishing

**Published online** 01, September, 2007

**Published in print edition** September, 2007

Nature has always been a source of inspiration and ideas for the robotics community. New solutions and technologies are required and hence this book is coming out to address and deal with the main challenges facing walking and climbing robots, and contributes with innovative solutions, designs, technologies and techniques. This book reports on the state of the art research and development findings and results. The content of the book has been structured into 5 technical research sections with total of 30 chapters written by well recognized researchers worldwide.

### **How to reference**

In order to correctly reference this scholarly work, feel free to copy and paste the following:

Li Chen, Yuechao Wang, Bin Li, Shugen Ma and Dengping Duan (2007). Study on Locomotion of a Crawling Robot for Adaptation to the Environment, Bioinspiration and Robotics Walking and Climbing Robots, Maki K. Habib (Ed.), ISBN: 978-3-902613-15-8, InTech, Available from:  
[http://www.intechopen.com/books/bioinspiration\\_and\\_robotics\\_walking\\_and\\_climbing\\_robots/study\\_on\\_locomotion\\_of\\_a\\_crawling\\_robot\\_for\\_adaptation\\_to\\_the\\_environment](http://www.intechopen.com/books/bioinspiration_and_robotics_walking_and_climbing_robots/study_on_locomotion_of_a_crawling_robot_for_adaptation_to_the_environment)

**INTECH**  
open science | open minds

### **InTech Europe**

University Campus STeP Ri  
Slavka Krautzeka 83/A  
51000 Rijeka, Croatia  
Phone: +385 (51) 770 447  
Fax: +385 (51) 686 166  
[www.intechopen.com](http://www.intechopen.com)

### **InTech China**

Unit 405, Office Block, Hotel Equatorial Shanghai  
No.65, Yan An Road (West), Shanghai, 200040, China  
中国上海市延安西路65号上海国际贵都大饭店办公楼405单元  
Phone: +86-21-62489820  
Fax: +86-21-62489821

© 2007 The Author(s). Licensee IntechOpen. This chapter is distributed under the terms of the [Creative Commons Attribution-NonCommercial-ShareAlike-3.0 License](#), which permits use, distribution and reproduction for non-commercial purposes, provided the original is properly cited and derivative works building on this content are distributed under the same license.